



Kinetics of zinc recovery from sphalerite in acetic acid solution

Ikechukwu Abuchi Nnanwube^{1*}, Judith Nkechi Udejaja²,
Okechukwu Dominic Onukwuli²

¹Chemical Engineering Department, Madonna University, Akpugo, Nigeria.

²Chemical Engineering Department, Nnamdi Azikiwe University, Awka, Nigeria

Received 22 Oct 2019,
Revised 30 Jan 2020,
Accepted 03 Feb 2020

Keywords

- ✓ Sphalerite,
- ✓ Kinetics,
- ✓ Acetic acid,
- ✓ Leaching,
- ✓ Zinc.

ik.nnanwube@gmail.com ;
Phone: +2348136140312;

Abstract

The kinetics of zinc recovery from sphalerite in acetic acid solution was investigated in this study. The effects of acid concentration, temperature, stirring rate, solid/liquid ratio and particle size on the leaching of sphalerite were investigated. Results of the leaching studies established that sphalerite dissolution in acetic acid solution increased with increasing concentration of acetic acid, temperature and stirring rate, and decreased with increasing particle size and solid/liquid ratio. The experimental data were analyzed by the shrinking core model (SCM), with the chemical reaction-controlled equation providing the best fitting; as demonstrated by the R^2 values of the models. The results further revealed a favorable leaching of the mineral with acetic acid with 86.6% recovery of zinc at the optimum conditions and with activation energy, Arrhenius constant and reaction constant values of 14.433 kJ/mol, 0.429 s⁻¹, and 44.871 s⁻¹, respectively.

1. Introduction

Sphalerite is a zinc sulphide mineral with a chemical composition of (Zn, Fe)S. Often found in metamorphic, igneous and sedimentary rocks in many parts of the world, sphalerite is the most commonly encountered zinc mineral and the world's most important ore of zinc. Dozens of countries have mines that produce sphalerite. Recent top producers include Australia, Bolivia, Canada, China, India, Ireland, Kazakhstan, Mexico, Peru, and the United States [1]. It is usually associated with other minerals, such as chalcopyrite, galena, pyrite, calcite, dolomite, and fluorite. It is of interest because of its semi-conducting properties, particularly since its band gap is in a region that leads itself to technological applications [2].

Zinc has found many applications as catalyst in organic synthesis including asymmetric synthesis, being cheap and easily available alternative to precious metal complexes. The results obtained by using chiral zinc catalysts are comparable to those achieved by palladium, ruthenium, iridium and others and therefore more and more zinc becomes metal of choice for this purpose [3]. One of the largest uses of zinc is in making protective coatings for steel. The development of the wide range of zinc coatings arose from two happy accidents of chemistry, the relatively slow and predictable rate of atmospheric corrosion of zinc compared with steel, and the relative positions of zinc and iron in the electrochemical series [4]. Zinc will corrode preferentially to give cathodic protection to iron when both are in contact in an aqueous medium. This is used to good effect to protect immersed structures such as ships' hulls, drilling rigs and

pipelines. It also means that any bare areas in a zinc coating on steel, caused by damage or operations such as cutting or drilling, are still protected by the surrounding zinc. Altogether, these two factors provide the basis of a unique corrosion protection system which uses some 4 million tonnes of zinc annually to protect around 100 million tons of steel. This represents almost half the total world consumption of zinc [4].

As the worldwide high grade ore reserves continue to deplete, hydrometallurgical route has been an alternative to pyrometallurgical processes for sulphidic ores and concentrates, particularly for small scale production and for remote metal resources not acceptable by pyrometallurgy [5]. In addition, the conventional roast-leach-electrolysis (RLE) process which can be seen as a combined pyrometallurgical and hydrometallurgical process generates SO₂, a major pollutant. The process is also not cost-effective due to other by-products and impurities that come with it [6-7].

A number of authors have studied hydrometallurgical routes for zinc extraction using acids and oxidative reagents. However, most of the leaching studies have been carried out using mainly inorganic acids such as hydrochloric acid [8-9], nitric acid [10-11] and sulphuric acid solutions [12]. In the present study, the effectiveness of an organic acid such as acetic acid as a leachant for the recovery of zinc from sphalerite is investigated. The experimental data were analyzed with the aid of the shrinking core model.

2. Material and Methods

2.1 Materials

Sphalerite sample obtained from Enyigba mining site, Abakaliki in Ebonyi state of Nigeria was used for this study. The ore sample was pulverized and sieved into five fractions: <75, 75-106, 106-212, 212-300, and <425 µm. All experiments were performed with <75 µm fraction except otherwise stated. Analytical grade reagents and deionized water were used to prepare all solutions.

2.2 Analytical methods

The chemical composition of the ore was determined with X-ray fluorescence spectroscopy (XRF) using X-supreme 60 oxford instruments. The mineralogical composition of the ore sample was determined by X-ray diffraction (XRD) with ARL X'TRA X-ray Diffractometer, Thermoscientific with the serial number 197492086 and Empyrean by PanAnalytical model using Cu K α radiation at 45kV and 40mA. The XRD patterns were recorded in the range of 5-65° 2 θ . The surface morphology of the ore was analyzed using Scanning electron microscopy (SEM) Q250 by FEI model from the Netherlands. The AAS analysis was conducted using Varian AA240 model.

2.3 Leaching procedure

For the leaching experiments, a 500 ml flat-bottomed flask was used. The glass was fitted with a condenser to prevent losses through evaporation. Heating was provided with the aid of a magnetically-stirred hot plate. The calculated volume of CH₃COOH solution was added to the flask, which was then heated to the desired temperature. Subsequently, a sample with a pre-determined weight was added to the reactor. At the end of each reaction time, the undissolved materials in the suspension was allowed to settle and separated by filtration. The resulting solutions were diluted and analyzed for zinc using atomic absorption spectrophotometer (AAS). Keeping other parameters constant, the effect of each parameter on the dissolution rate was evaluated. The post-leached residues after dissolution in the optimum conditions were subjected to SEM and XRD examination [11].

2.4 AAS analysis

AAS analysis was conducted according to the method of American Public Health Association (APHA) 1995 [13]. Atomic absorption spectrometer's working principle is based on the sample being aspirated into the flame and atomized when the AAS's light beam is directed through the flame into the monochromator, and unto the detector that measures the amount of light absorbed by the atomized element in the flame. Since metals have their own characteristic absorption wavelength, a source lamp composed of that element is used, making the method relatively free from spectral or radiational interferences. The amount of energy of the characteristic wavelength absorbed in the flame is proportional to the concentration of the element in the sample.

Procedure: The sample was thoroughly mixed by shaking, and 100 ml of it was transferred into a glass beaker of 250 ml volume, to which 5 ml of concentrated nitric acid was added and heated to boil till the volume was reduced to about 15-20 ml, by adding concentrated nitric acid in increments of 5 ml till all the residue was completely dissolved. The mixture was cooled, transferred and made up to 100 ml using metal-free distilled water. The sample was aspirated into the oxidizing air-acetylene flame. When the aqueous sample was aspirated, the sensitivity for 1% absorption was observed. The reference solution was prepared daily by diluting the single stock zinc solution (which had been prepared in the optimum concentration range) with water containing 1.5 ml concentrated nitric acid per litre. A calibration blank was prepared using all the reagents except for the metal stock solution. Calibration curve for zinc was prepared by plotting the absorbance of standard versus zinc concentration.

3. Results and discussion

3.1 Characterization

The results of the chemical analysis of the sphalerite sample had earlier been reported [11]. The result as shown in Figure 1 revealed that ZnO, SO₃, Na₂O and Fe₂O₃ were the major oxides present in the ore; oxides such as SiO₂, CaO, Al₂O₃, Mn₂O₃ and MgO were present in minor quantities while the rest occurred in traces.

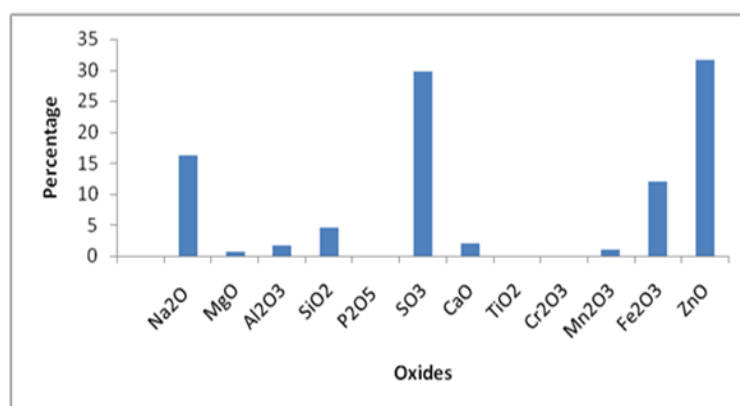


Figure 1: XRF result of Enyigba sphalerite.

Table 1 presents the results of the X-ray diffractogram of Enyigba sphalerite with important compounds identified. The result revealed the presence of sphalerite as the dominant mineral with three major peaks at 3.12, 1.91 and 1.63 Å, respectively, and cerium germanium sulphide (Ce₂GeS₂) as an associated mineral with three major peaks at 2.96, 2.09 and 3.42 Å, respectively as shown in Figure 2. The data for other peaks are shown in Table 1.

Table 1. The X-ray diffraction data of the sphalerite showing the angle 2θ and d-values of the compounds identified, with their relative intensity (%) [11].

2θ	d-Value (Å)	Compound	Intensity (%)	JCPDS file No.
26.03	3.42	Cerium Germanium Sulphide (Ce_2GeS_2)	45.95	03-065-8125
28.56	3.12	Sphalerite (ZnS)	100.00	03-065-9585
30.15	2.96	Cerium Germanium Sulphide (Ce_2GeS_2)	100.00	03-065-8125
33.09	2.70	Sphalerite (ZnS)	8.71	03-065-9585
43.16	2.09	Cerium Germanium Sulphide (Ce_2GeS_2)	63.86	03-065-8125
47.50	1.91	Sphalerite (ZnS)	50.45	03-065-9585
51.09	1.79	Cerium Germanium Sulphide (Ce_2GeS_2)	17.62	03-065-8125
53.54	1.71	Cerium Germanium Sulphide (Ce_2GeS_2)	19.72	03-065-8125
56.37	1.63	Sphalerite (ZnS)	26.00	03-065-9585
59.11	1.56	Sphalerite (ZnS)	1.70	03-065-9585

JCPDS File No. : Joint Committee on Power Diffraction Standards File Number.

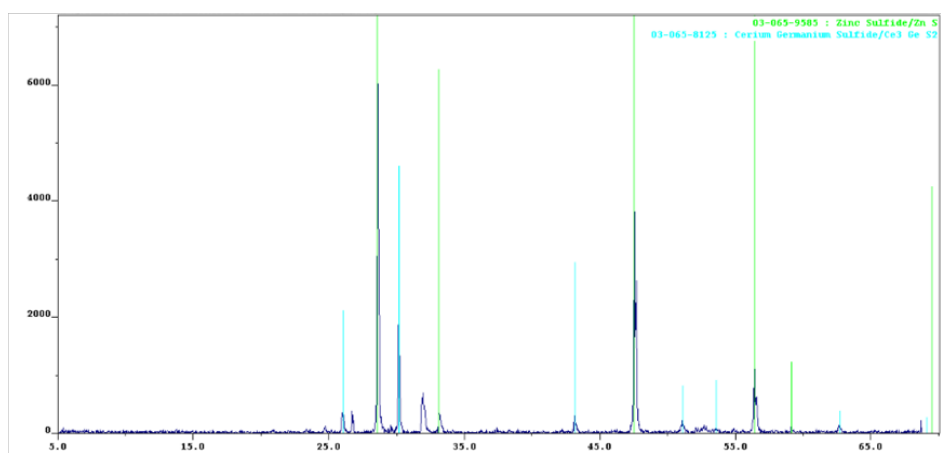


Figure 2: X-ray diffraction pattern of Enyigba sphalerite.

The scanning electron micrograph (SEM) of sphalerite is presented in Figure 3 with magnifications of 500x, 1000x and 1500x, respectively. The results indicate that the particles are very cohesive, confirming their micrometer sized agglomerates with irregular shapes and rough edges and form microscopic flakes. Similar results were obtained by Onukwuli and Nnanwube [11].

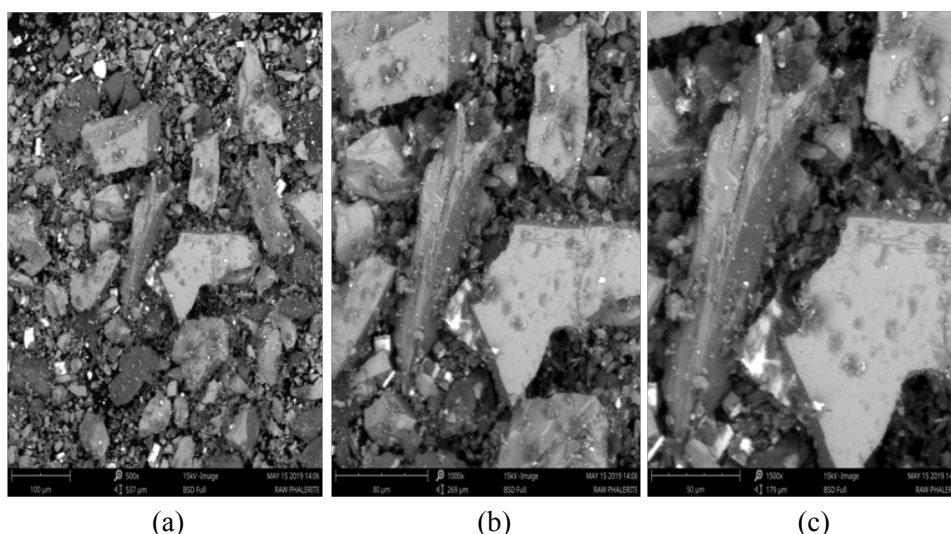


Figure 3: SEM images of sphalerite ore showing magnifications of 500× (a), 1000× (b) & 1500× (c), respectively.

3.2 Effect of process parameters on leaching rate

3.2.1 Effect of CH_3COOH concentration on sphalerite dissolution

The results of the effect of CH_3COOH concentration on sphalerite dissolution are illustrated in Figure 4. The results show that the fraction of sphalerite dissolved increased with increasing acid concentration and leaching time. The results obtained with 12 M CH_3COOH at 150 minutes leaching time (84.6wt %) was slightly lower compared to that obtained with 10 M CH_3COOH (85.1wt %), and this could be attributed to a change in the rate determining step due to the significant quantity of elemental sulphur produced. This agrees with the results obtained by Warren et al. [14]. Hence, 10 M CH_3COOH was used for further studies.

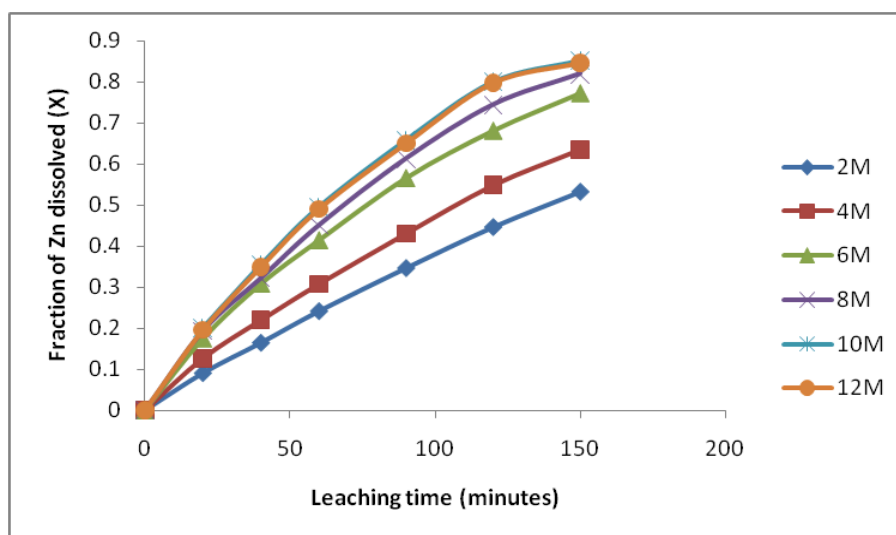


Figure 4: Effect of CH_3COOH concentration on sphalerite dissolution at various leaching time. *Experimental conditions:* particle size = $<75 \mu\text{m}$; solid/liquid ratio = 20g/L; temperature = 333K; stirring speed = 400 rpm.

3.2.2 Effect of stirring rate on sphalerite dissolution

The results on the effect of stirring rate on sphalerite dissolution in 10M CH_3COOH over the range of 100-600 rpm at 363K is presented in Figure 5. The results show that the amount of sphalerite dissolved increased with increase in leaching time. Figure 5 shows that the amount of sphalerite dissolved is dependent on the stirring speed over the range 100-500 rpm. Above 500 rpm, the stirring speed did not have any substantial effect on the ore dissolution. Hence dissolution reached a steady rate at 500 rpm, and a stirring speed of 500 rpm was retained for further studies.

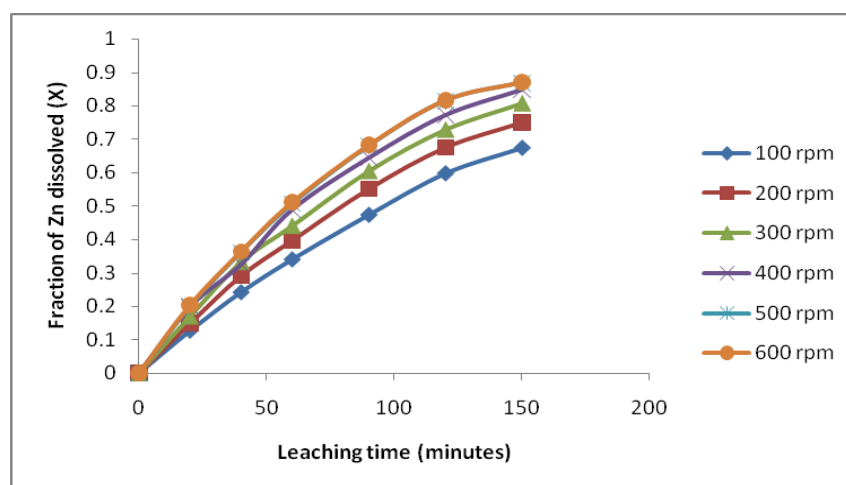


Figure 5: Effect of stirring rate on sphalerite dissolution at various leaching time. *Experimental conditions:* particle size = $<75 \mu\text{m}$; solid/liquid ratio = 20g/L; temperature = 363K; CH_3COOH concentration = 10M.

3.2.3 Effect of temperature on sphalerite dissolution

The effect of temperature on sphalerite dissolution has been investigated over the temperature range 323-363K in 10 M CH₃COOH solution at a stirring rate of 500 rpm using 75 μ m particle diameter and solid/liquid ratio of 20 g/L. These results are presented in Figure 6. From Figure 6, sphalerite dissolution increased with increase in leaching time and with increasing temperature. The results obtained here agree with the results of Baba and Adekola [8]. At 363K, the amount of sphalerite dissolved within 150 min was 86.8%.

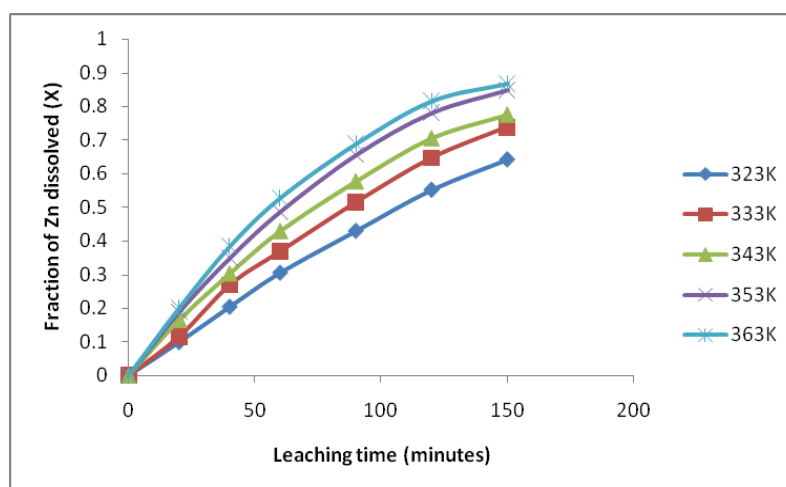


Figure 6: Fraction of sphalerite dissolved against leaching time at different temperatures. *Experimental conditions:* particle size = <75 μ m; solid/liquid ratio = 20g/L; stirring rate = 500 rpm; CH₃COOH conc. = 10M.

3.2.4 Effect of solid/liquid ratio on sphalerite dissolution

The results on the effect of solid/liquid ratio on sphalerite dissolution in 10 M CH₃COOH were investigated in the range 0.02 to 0.045 g/ml at a temperature of 363K. The results show that the amount of sphalerite dissolved increased with increase in leaching time. Figure 7 shows the effect of solid/liquid ratio on sphalerite dissolution in 10 M CH₃COOH. Decreasing the solid/liquid ratio is accompanied with increase in the equilibrium percentage of the ore dissolved. For instance, by varying the solid/liquid ratio from 0.045 to 0.02 g/ml, the percentage of sphalerite dissolved increased from 56.8% to 86.4% after a leaching time of 150 minutes. This could be attributed to the decrease in the fluid reactant per unit weight of the solid. This agrees with the results of Onukwuli and Nnanwube [11].

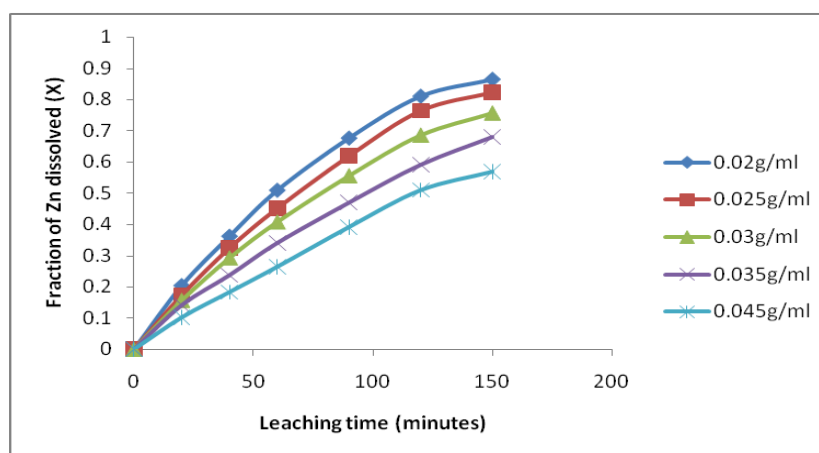


Figure 7: Effect of solid/liquid ratio on sphalerite dissolution. *Experimental conditions:* CH₃COOH concentration = 10 M; particle diameter = <75 μ m; stirring rate = 500 rpm; temperature = 363K.

3.2.5 Effect of particle size on sphalerite dissolution

The influence of particle diameter on sphalerite dissolution in CH₃COOH was investigated for five different sized fractions. The results are summarized in Figure 8. The figure shows that the amount of sphalerite dissolved increased with increase in leaching time. The results from Figure 8 showed that the smaller the sphalerite particle

size, the faster was the sphalerite dissolution. This is due to the large contact surface area between the sphalerite particles and the leachant. This agrees with the results of Baba and Adekola [8]. This observation was also supported by Aydogan et al. [15].

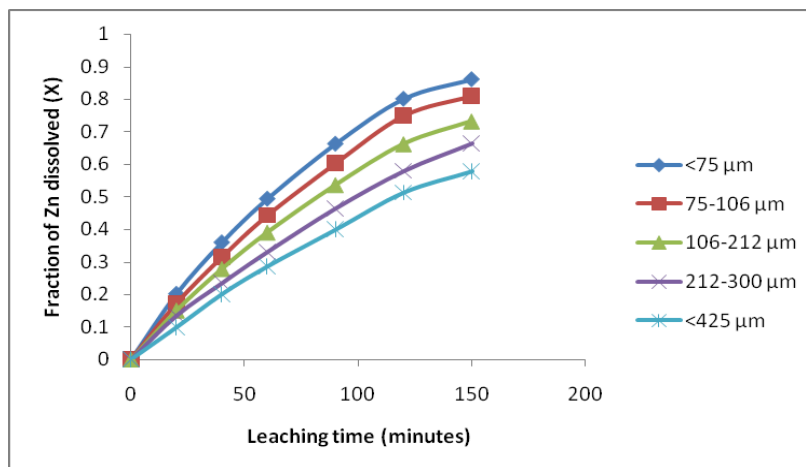


Figure 8: Effect of particle diameter on sphalerite dissolution. *Experimental conditions*: CH₃COOH concentration = 10 M; solid/liquid ratio = 20 g/L; stirring rate = 500 rpm; temperature = 363K.

3.3 Kinetic analysis

For this study, the shrinking core models were tested for better understanding of the dissolution of sphalerite in CH₃COOH media. The kinetic models have been previously utilized by some authors such as Aydogan et al. [15-16], Baba and Adekola [8], Habashi [17], Khalique et al. [18], Leao [19], and Ajemba [20].

Equation (1) is applicable to a chemical reaction controlled process at the interface. This is the opposite of the diffusion controlled mechanism since the rate of chemical reaction is much slower than the rate of diffusion and this process strongly depends on temperature since the rate of chemical reaction increases with temperature. Equation (2) is applicable to a diffusion-controlled process through the product layer. This type of process is characterized by a slight dependence on temperature since the rate-determining step is almost independent of temperature. It has a strong dependence on agitation speed since it increases the thickness of the boundary layer [21]. Equation (3) is a mixed-controlled process (a combination of surface reaction and diffusion).

$$1-(1-X)^{1/3} = \frac{bk_s C_A t}{\rho_s r_o} = k_2 t \quad (1)$$

$$1+2(1-X) - 3(1-X)^{2/3} = \frac{6bD_e C_A t}{\rho_s r_o^2} = k_3 t \quad (2)$$

$$1-(1-X)^{1/3} + (y/6)[(1-X)^{1/3} + 1 - 2(1-X)^{2/3}] = k_4 t \quad (3)$$

A modified form of the shrinking core model for product ash layer diffusion control was developed by Ginstling and Brounshtein [22] as shown in Equation (4).

$$1 - (2/3)X - (1-X)^{2/3} = k_5 t \quad (4)$$

where X is the fraction of the metal dissolved at time t, b the stoichiometric coefficient of the reagent in the leaching reaction, k_s the kinetic constant, C_A the concentration of the lixiviant, ρ_s the density of the solid, r_o the initial radius of the solid, and k_2 the rate constant from Equation (1). D_e is the effective diffusion coefficient, k_3 , k_4 and k_5 are the rate constants for Equations (2), (3) and (4), respectively; y is taken to be 1 for heterogeneous systems. Of all the four models tested, the experimental data were found to fit the relation in Equation (1) with an ideal correlation of about 0.99. The analysis of the plots of other kinetic curves gave lower correlation coefficients. Hence, the linearization of Figures 4 – 8 was made and from the data in Figure 4, the expression: $1 - (1 - X)^{1/3} = k_1 t$, gave an average correlation coefficient of 0.997 and this is shown in Figure 9.

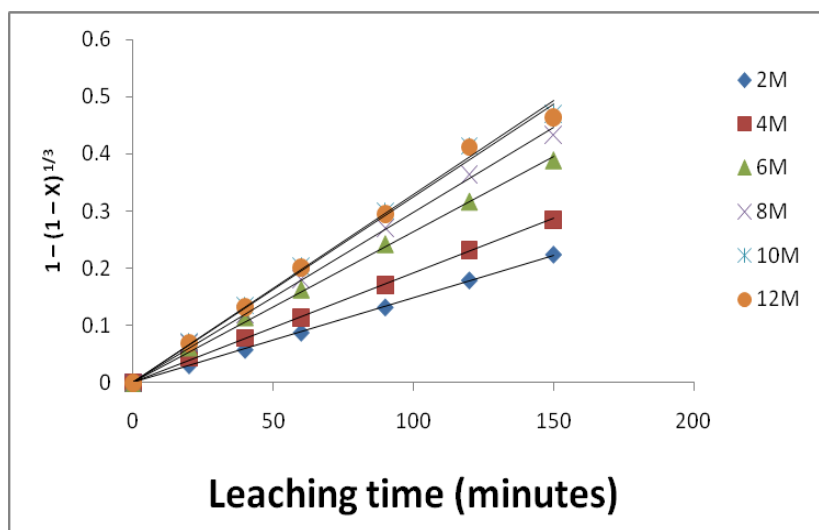


Figure 9: Plot of $1 - (1-X)^{1/3} = kt$ against leaching time at various CH_3COOH concentrations for data presented in Figure 4.

From Figure 9, the experimental rate constant k_1 , was calculated from the slope of the straight line at various CH_3COOH concentrations and the plots of $\ln k_1$ versus $\ln (\text{CH}_3\text{COOH})$ are shown in Figure 12a. From Figure 12a, the slope of the resulting plot gave 0.476. This shows that the order of reaction with respect to CH_3COOH is 0.476 with correlation coefficient of 0.971. The results presented in Figure 6 at different k_6 temperatures were linearized by Equation (1) and presented in Figure 10. Likewise, the apparent rate constant k_6 was calculated from the slope of the straight line at various stirring rates (w). The plot of $\ln k_6$ against $\ln w$ is shown in Figure 12b. The data in Figures 7 and 8 were additionally linearized by means of Equation (1).

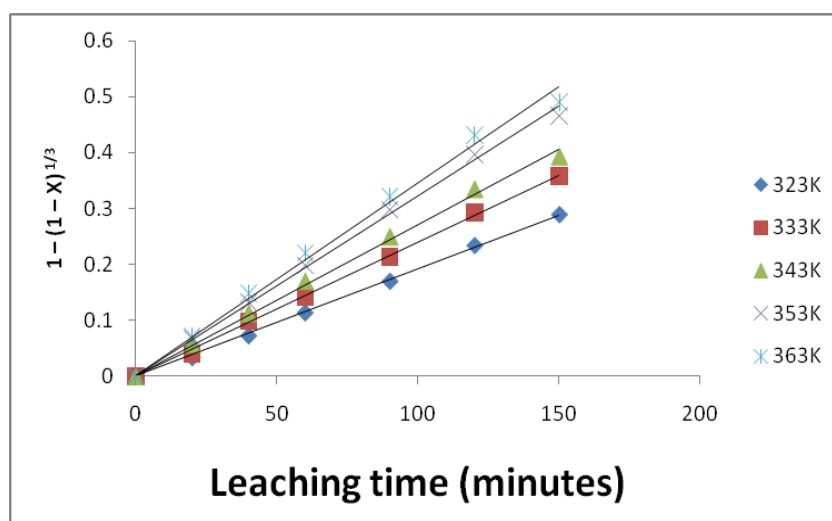


Figure 10: Plot of $1 - (1-X)^{1/3} = kt$ against leaching time at various temperatures for data presented in Figure 6.

From Figure 10, the apparent rate constants, k_2 , and other tested constants, k_3 , k_4 and k_5 were determined from the slopes of the straight lines. The estimations of these rate constants with their proportional correlation coefficients are presented in Table 2. Using the rate constants derived from the slopes in Figure 10, the Arrhenius diagram in Figure 11 was plotted from which the activation energy of 14.433 kJ/mol was determined. The Arrhenius constant for the process was estimated to be 0.429 s^{-1} with a correlation coefficient (R^2) of 0.981. The activation energy calculated for this study appears to be the lowest compared to other reported works as summarized in Table 3. The sphalerite mineral obtained from Abakaliki can therefore be said to be kinetically more favorable to leaching by CH_3COOH compared to other sphalerite types.

Table 2: Values of the rate constants and regression coefficients for sphalerite dissolution in 10 M CH_3COOH

Temperature (K)	Apparent rate constant ($\times 10^{-3} \text{ min}^{-1}$)				Correlation coefficient (R^2)			
	K_2	K_3	K_4	K_5	k_2	k_3	k_4	k_5
323	1.92	1.12	2.73	0.375	0.999	0.888	1.000	0.888
333	2.40	1.66	3.37	0.553	0.999	0.904	0.998	0.901
343	2.71	2.03	3.78	0.675	0.997	0.931	0.992	0.931
353	3.23	2.71	4.43	0.904	0.997	0.935	0.992	0.936
363	3.46	3.02	4.72	1.010	0.993	0.946	0.984	0.947

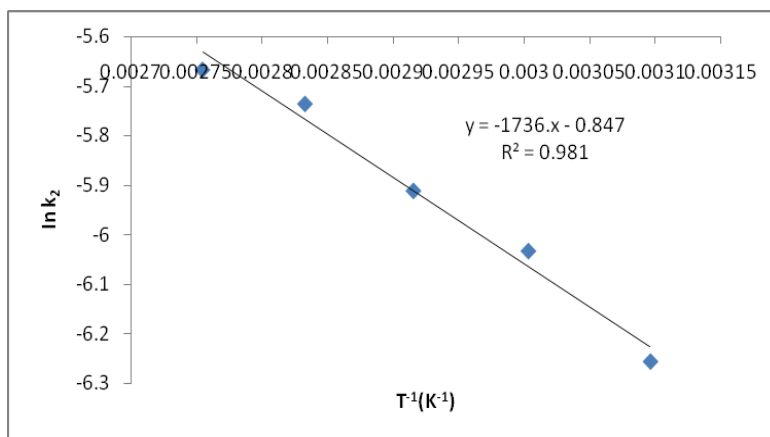


Figure 11: Arrhenius plot of reaction rate against reciprocal of temperature.

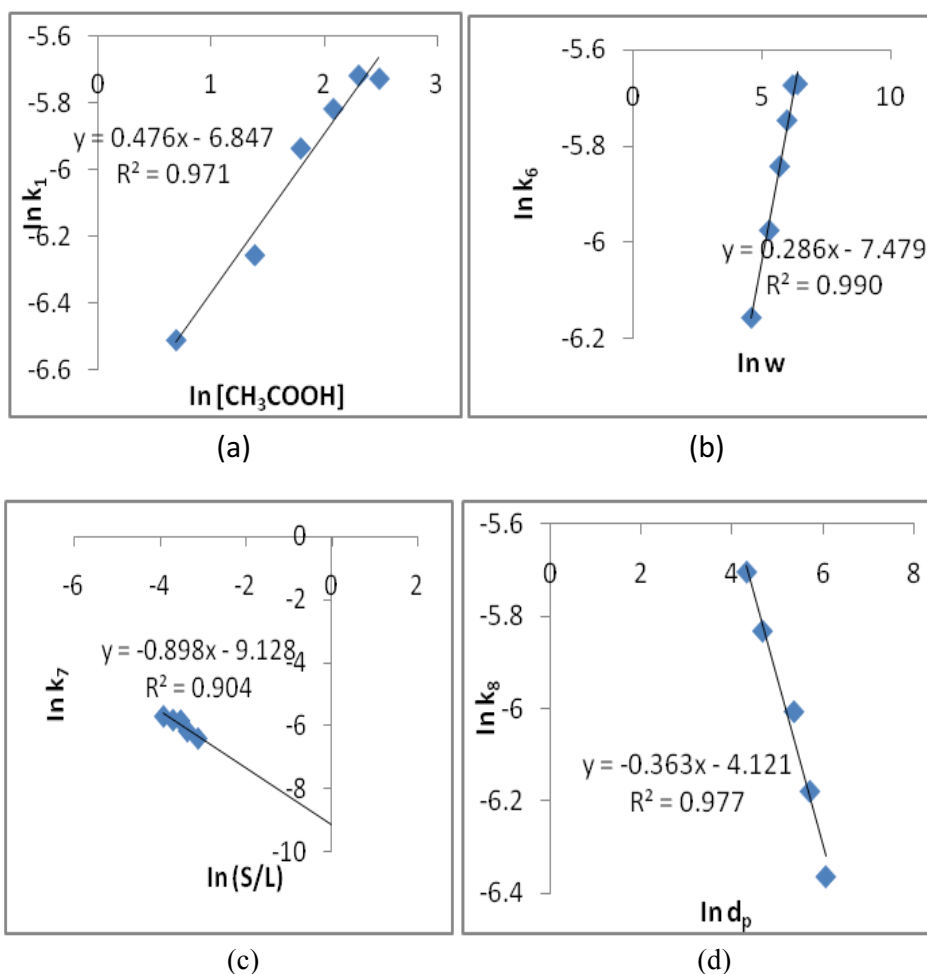


Figure 12: Plots to determine order of acid concentration (a), stirring rate (b), S/L ratio (c), and particle size (d).

Table 3: Some reported activation energies for sphalerite leaching by different leaching systems.

Origin of sphalerite	Leachant	Ea (kJ/mol)	References
Bhubaneswar, India	4 M HCl/1 M MnO ₂	56.7	Madhuchanda et al.[23]
Sivas, Turkey	0.25 M FeCl ₃ /0.1 M HCl	45.3	Aydogan et al. [24]
Pittsburgh, China	0.2 M FeCl ₃ /0.1 M HCl	58.4	Zuo-mei et al. [25]
Abakaliki, Nigeria	10M HNO ₃	26.4	Onukwuli and Nnanwube [11]
Abakaliki, Nigeria	10M CH ₃ COOH	14.43	This study

3.3.1 Dissolution model

From the effects of the solid/liquid ratio (Figure 7) and particle diameters (Figure 8) on sphalerite dissolution in 10M CH₃COOH solution, the apparent rate constants, k_7 and k_8 were evaluated, respectively. The solid/liquid ratio and initial particle size (d_p) were found to be inversely proportional to 0.898 power $(S/L)^{-0.898}$ and 0.363 power ($d_p^{-0.363}$) as shown in Figures 12 (c and d). Hence, the proposed model equation for sphalerite dissolution by 10M CH₃COOH solution at 363K is consistent with the following relation (Equation 5):

$$1 - (1-X)^{1/3} = k_o C_{CH_3COOH}^{0.476} (d_p)^{-0.363} (\rho \frac{S}{L})^{-0.898} (w)^{0.286} e^{(-14433.1/RT)} t \quad (5)$$

where ρ is the ore density, k_o is a reaction constant, which can be determined from the fraction of sphalerite dissolved, X at a given time, t. The parameter, X is determined experimentally. For instance, at 363K, the value of X = 0.866 (86.6% dissolution); k_o is calculated to be 44.871 s⁻¹. The value of k_o , however, is found to vary depending on the leaching systems/conditions [8].

3.4 Characterization of the residual product

3.4.1 SEM analysis of sphalerite leached with 10M CH₃COOH

The morphology of sphalerite after leaching with 10M CH₃COOH was examined with by scanning electron micrograph (SEM) and obtained with magnifications of 500×, 1000× and 1500×, respectively, as shown in Figure 13. The micrographs of the leaching residues show a progressive increase in the roughness of the solid and also an increase in the amount of elemental sulphur covering the particle surfaces. Similar results were obtained by Souza et al. [26]. The particles have irregular shapes and form microscopic flakes and may be poorly crystalline due to attack by the lixiviant.

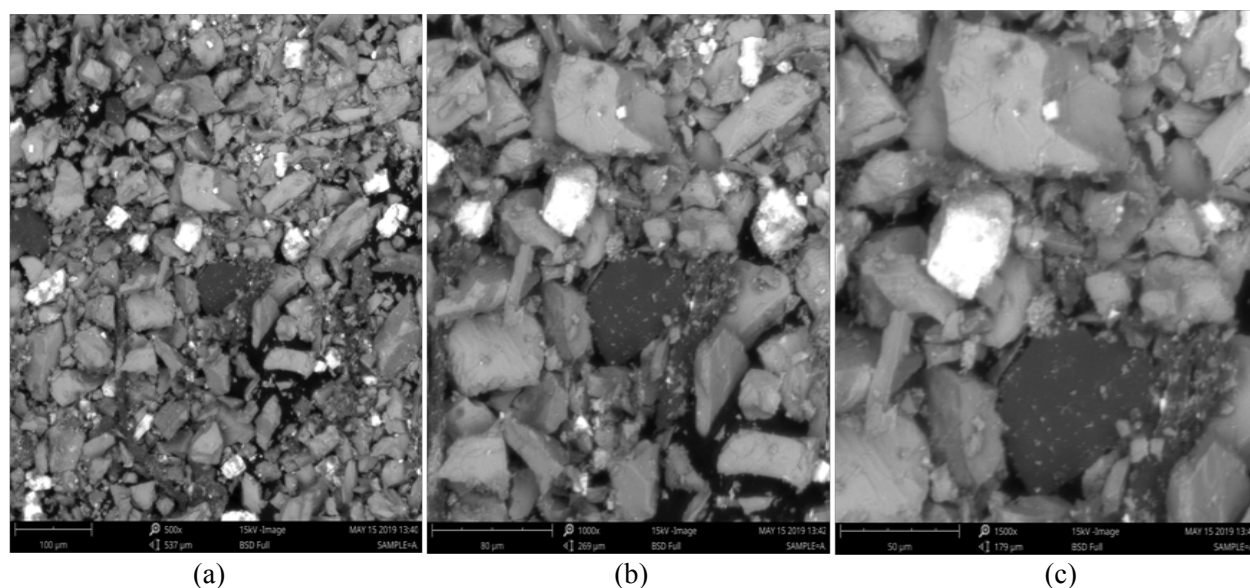


Figure 13: SEM image of sphalerite leached with 10M CH₃COOH with magnifications of 500× (a), 1000× (b), 1500× (c), respectively.

3.4.2 XRD analysis of sphalerite leached with 10 M CH₃COOH

The analysis of sphalerite leached with 10M CH₃COOH at 363K by X-ray diffraction gives a description of the mineral phases present in the residue. Table 4 presents the results of the X-ray diffractogram of the residue. The result showed the presence of sphalerite with three major peaks at 3.12, 1.91, and 1.63 Å, respectively as well as the presence of galena with three major peaks at 2.97, 3.43, and 2.10 Å, respectively, as shown in Figure 14. Other peaks are shown in Table 4.

Table 4: The X-ray diffraction data of the sphalerite leached with 10M CH₃COOH showing the angle 2θ and d-values of the compounds identified, with their relative intensity (%).

2θ	d-Value (Å)	Compound	Intensity (%)	JCPDS file No.
28.56	3.12	Sphalerite (ZnS)	100.0	96-900-0108
33.10	2.70	Sphalerite (ZnS)	9.4	96-900-0108
47.51	1.91	Sphalerite (ZnS)	58.9	96-900-0108
56.37	1.63	Sphalerite (ZnS)	37.1	96-900-0108
59.12	1.56	Sphalerite (ZnS)	2.2	96-900-0108
25.98	3.43	Galena (PbS)	91.9	96-900-8695
30.09	2.97	Galena (PbS)	100.0	96-900-8695
43.07	2.10	Galena (PbS)	72.8	96-900-8695
50.99	1.79	Galena (PbS)	45.0	96-900-8695
53.43	1.71	Galena (PbS)	25.1	96-900-8695

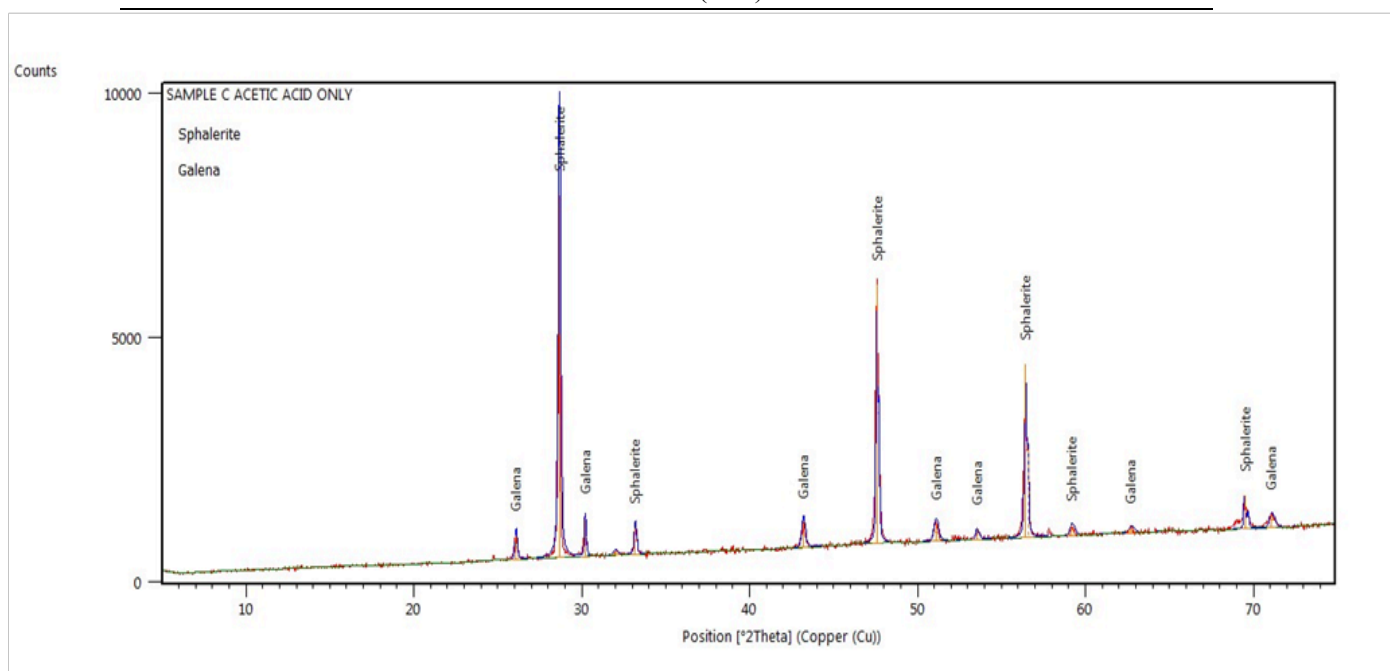


Figure 14: XRD pattern of sphalerite leached with 10M CH₃COOH.

Conclusion

The effectiveness of acetic acid as leachant for recovering zinc from sphalerite was investigated in this study. The leaching investigation showed clearly that sphalerite dissolution in acetic acid solution increased with increasing concentration of acetic acid, temperature and stirring rate, and decreased with increasing particle diameter and solid/liquid ratio. In 10M CH₃COOH at a temperature of 363K using <75µm particle diameter with solid/liquid ratio of 20g/L and stirring speed of 500 rpm, about 86.6% of sphalerite dissolved in 150 minutes. The values of activation energy, order of reaction and Arrhenius constant were estimated as 14.43 KJ/mol, 0.476, and 0.429 s⁻¹,

respectively. The results of the dissolution studies indicated that the experimental data fitted the chemical reaction-controlled equation of the shrinking core model. In general, acetic acid was found to be effective for the leaching process.

References

1. M. Frenzel, M.P. Ketris, T. Seifert, J. Gutzmer, On the current and future availability of gallium, *Resources Policy*, 47 (2016) 38-50. <https://doi.org/10.1016/j.resourpol.2015.11.005>
2. L. Cao, S. Huang, E. Shulin, ZnS/CdS/ZnS quantum dot quantum well produced in inverted micelles. *Journal of Colloid and Interface Science*, 273(2004) 478-482. <https://doi.org/10.1016/j.jcis.2004.02.031>
3. D. Lowicki, S. Bas, J. Mlynarski, Chiral zinc catalysts for asymmetric synthesis, *Tetrahedron*, 71 (2015) 1339-1394. <https://doi.org/10.1021/acs.jmedchem.9b01104>
4. A. Wall, Zinc and its uses, *Materials World*, 6 (1998) 1-5.
5. K. Rotuska, T. Chmielewski, Growing role of solvent extraction in copper ores processing, *Physicochemical Problems of Mineral Processing*, 42 (2008) 29-36.
6. E. Guler, Pressure acid leaching of sphalerite concentrate: modeling and optimization by response surface methodology, *Physicochemical Problems of Mineral Processing*, 52(1)(2016)479-496. <https://doi.org/10.5277/ppmp19023>
7. M. Hasani, S.M.J. Koleini, A. Khodadadi, Kinetics of sphalerite leaching by sodium nitrate in sulphuric acid”, *Journal of Mining and Environment*, 7(1)(2016)1–12. <http://doi:10.22044/jme.2016.454>
8. A.A. Baba, F.A. Adekola, Hydrometallurgical processing of a Nigerian sphalerite in hydrochloric acid: Characterization and dissolution kinetics, *Hydrometallurgy*, 101 (2010)69 – 75. <https://doi.org/10.1016/j.hydromet.2009.12.001>
9. G. Ucar, Kinetics of sphalerite dissolution by sodium chlorate in hydrochloric acid, *Hydrometallurgy*, 95(2009) 39 – 43. <https://doi.org/10.1179/1879139512Y.0000000001>
10. A.O. Adebayo, K.O. Ipinmoroti, O.O. Ajayi, Leaching of sphalerite with hydrogen peroxide and nitric acid solutions, *Journal of Minerals & Materials Characterization & Engineering*,5 (2006) 167 – 177. <https://doi.org/10.4236/jmmce.2006.52012>
11. O.D. Onukwuli, I.A. Nnanwube, Hydrometallurgical processing of a Nigerian sphalerite ore in nitric acid: Characterization and dissolution Kinetics, *The International Journal of Science and Technoledge*, 6 (2018) 40-54.
12. P.A. Olubambi, J.O. Borode, S. Ndlovu, Sulphuric acid leaching of zinc and Copper from Nigerian complex sulphide ore in the presence of hydrogen peroxide, *The Journal of the Southern African Institute of Mining and Metallurgy*, 106 (2006) 765-770.
13. American Public Health Association 3112B, Cold-Vapour Atomic Spectrometric Method, Standard Methods for the Examination of Water and Wastewater, 20th Edition, APHA, AWWA, WEF (1995).
14. G.W. Warren, S. kim, H. Henein, The effect of chloride ion on the ferric chloride leaching of galena concentrate, *Metall. Mater. Trans. B.*, 15B (1987) 59 - 69. <http://dx.doi.org/10.14288/1.0078519>
15. S. Aydogan, M. Erdemoglu, G. Ucar, A. Aras, Kinetics of galena dissolution in nitric acid solutions with hydrogen peroxide, *Hydrometallurgy*, 88 (2007a) 52-57. <https://doi.org/10.1016/j.hydromet.2007.03.005>
16. S. Aydogan, M. Erdemoglu, G. Ucar, A. Aras, Dissolution kinetics of galena in acetic acid solutions with hydrogen peroxide, *Hydrometallurgy*, 89(2007b)189-195. <https://doi.org/10.1016/j.hydromet.2007.07.004>
17. F. Habashi, Hydrometallurgy of lead, *Metallurgia*, 59 (2005) 114 -118.
18. A. Khalique, A. Akram, A.S. Ahmed, N. Hamid, Effect of sodium chloride on dissolution of galena in aqueous acid solution, *Pak. J. Sci. Ind. Res.*,48 (2005) 236 – 239.
19. V.A. Leao, A.D. Souza, P.S. Pina, C.A. Silva, P.F. Siqueira, The leaching kinetics of zinc sulphide concentrate in acid ferric sulphate, *Hydrometallurgy*, 89 (2007) 72 – 81. <https://doi.org/10.1016/j.hydromet.2007.05.008>

20. R.O. Ajemba, Thermodynamics and kinetic modeling of the dissolution and adsorptive applications of Ukpok, Udi and Nteje clays, Ph.D Thesis, Nnamdi Azikiwe University, Awka, Anambra, Nigeria, (2012). http://naulibrary.org/dglibrary/admin/book_directory/Thesis/11051.pdf
21. F.A. Habashi, *Textbook of hydrometallurgy, 1st ed.*, Sainte Foy, Quebec: Metallurgie Extractive Quebec, (1993).
22. A.M. Ginstling, V.I. Brounshtein, The diffusion kinetics of reaction in spherical particle, *J. Appl. Chem.*, 23(1950) 1327 – 1338.
23. M. Madhuchhanda, N.B. Devi, K.S. Rao, P.C. Rath, R.K. Paramguru, Oxidation of sphalerite in hydrochloric acid medium in the presence of manganese dioxide. *Inst. Min. Metall.*, 109 (2000) 150-155.
24. S. Aydogan, A. Aras, M. Cambazoglu, Dissolution kinetics of sphalerite in acidic ferric chloride leaching, *Chemical Engineering Journal*, 114(2005) 67-72. <https://doi.org/10.1016/j.cej.2005.09.005>
25. J. Zuo-mei, G.W. Warren, H. Henein, Reaction kinetics of ferric chloride leaching of sphalerite: an experimental study, *Metallurgical Transactions B.*, 15B(1984) 5 -12.
26. A.D. Souza, P.S. Pina, V.A. Leao, Bioleaching and chemical leaching as an integrated process in the zinc industry, *Minerals Engineering*, 20(2007) 591 – 599. <https://doi.org/10.1016/B978-0-12-804022-5.00001-3>

(2020) ; <http://www.jmaterenvirosci.com>